Scaled UAV Prototyping and Control

João Ornelas
joao.camara.ornelas@tecnico.ulisboa.pt

Instituto Superior Técnico, Universidade de Lisboa, Portugal

October 2021

Abstract

The Flexcraft project in which this work is included, aims to design a modular aircraft with a removable fuselage, in collaboration between Instituto Superior Técnico and several companies including AlmaDesign, SETsa, Embraer Portugal and INEGI. A model aircraft was then built and tested with a scale factor of one to ten, in order to investigate the potential advantages and disadvantages of the chosen configuration and gain more experience in this type of non-conventional aircraft configuration. Additionally, this work proposes the implementation of a control system in the scaled unmanned aerial vehicle with the tuning of the control system based on parameters determined through simulation and experimental measurements. This process consists of modeling the F02 aircraft, using tools such as MATLAB and SIMULINK. The control system is also modelled in the same software and controller gains are obtained by applying PID feedback linear control techniques to the linearized aircraft model and tested on the non-linear model. Finally, a flight was performed to measure the behaviour of the real prototype and try to draw conclusions about the feasibility of this configuration and what future work can be done using the prototype built as a test platform.
Keywords: Unmanned Aerial Vehicle, Dynamic Modelling, PID Control, Manufacturing Project.

1. Introduction

Advances in aeronautical engineering have been continually assisted with the development of better analysis and design tools, that have been used in the early design stages of a new aircraft [1]. These methods have provided data and understanding of the physical phenomenons involved and enabled designers to predict, analyse, and change the characteristics of new vehicles to more suitable and advantageous ones. One of these tools since the earliest flights has been testing on a sub-scale model. The first individuals to use this tool were Leonardo da Vinci, George Cayley, and the Wright brothers to better understand and design their flying machines. Models are now frequently used as a key element in new aerospace research and development programs, they are used in many applications and roles, including aerodynamic data gathering in wind tunnel investigations, for the analysis of full-scale aircraft design or proof-of-concept demonstrators for radical aeronautical concepts [1].

With this information in mind, a scaled Unmanned Aerial Vehicle (UAV) is built to be used as a test platform to research the viability of the proposed aircraft of the Flexcraft project with an electric propulsion system to emulate its hybrid system.

1.1. Project Flexcraft

Beginning in December 2016, the project Flexcraft, consists of a consortium of various companies and Portuguese institutions to demonstrate the country's capacity for the implementation and development of an innovative system and its future application in the aeronautical sector. The consortium consists of five entities, AlmaDesign, SETsa, Embraer Portugal, INEGI and Instituto Superior Técnico [2].

The designation attributed to the aircraft, Flexcraft, as the name implies, aims to represent its adaptability for a wide spectrum of differentiated missions in an expeditious and flexible way, by having several modular and detachable fuselages that can be designed specifically to each mission. These research lines will be validated through three evolutionary demonstrators, namely, with the construction of two UAVs, one on a scale 1 by 10 and one 1 by 15, a scalar mock-up and demonstrators of materials and production processes [3] [4]. The main focus of this work will focus on the control and construction of the 1 by 10 scale model of the original aircraft.

1.2. Objectives

The purpose of this work is to build and test a scaled model with a scale ratio of 1:10, as a proof of concept of the proposed aircraft that will also be

controlled by a linear controller designed for this project. To set up this controller, a computational model of the scaled model is set as a goal, and the required parameters are estimated or measured. In the next phase, the controller is modelled and by including the model at this point, it is possible to tune the proposed controller. Finally, a flight test is produced to try to get some conclusions about this aircraft concept.

2. Background

To build this model, we start with the assumption of a rigid body physics with no flexible body parts that could be added but introduces several complexities that generally do not have a big impact on the type of controllers to be designed. The motion of the aircraft is then the sum of all the forces exerted on the center of mass from the propulsion, aerodynamics or gravity itself.

2.1. Kinematics

Kinematics represents the study of movement, discarding the causes of said movement. The representation of the movement of the rigid body is then described by a three-dimensional vector in relation to a given reference frame, and it is necessary to define at least two coordinate references, the inertial frame and the body frame.

It was defined as an inertial frame, one where its origin is on the Earth's surface, in the initial position of the body before its movement, this frame is often called the NED frame, with the x-axis pointing to the North, the y-axis to the East, and the z to the interior of the Earth (Down). It is worth noting that we can assume this is an inertial reference because the solid body has a maximum speed well below the Earth's rotation speed, the same can not be ignored for long or high velocity flights.

The body has the x-axis pointing forward in relation to the vehicle, aligned with its plane of symmetry, the y-axis is perpendicular to it, pointing to the right side of the vehicle. Finally, the z-axis points downward in order to satisfy the right-hand rule.

2.1.1. Coordinate system transformation

We need to define a transformation between the two frames. This operation is usually performed using Euler or Quaternion angles. Using Euler angles, this operation is described with three successive rotations, represented by each of the Euler angles. Mathematically, the NED to body coordinate system is transformed through the following matrix multiplication:

$$\mathbf{C}_{bE} = \begin{bmatrix} c\theta c\psi & c\theta s\psi & -s\theta \\ (-c\phi s\psi + s\phi s\theta c\psi) & (c\phi c\psi + s\phi s\theta s\psi) & s\phi c\theta \\ (s\phi s\psi + c\phi s\theta c\psi) & (-s\phi c\psi + c\phi s\theta s\psi) & c\phi c\theta \end{bmatrix} \quad (1)$$

The rotation matrix from the body coordinate system to the NED frame will be the inverse matrix of C_{bE}, called C_{Eb}. Furthermore, in the simulation, the evolution of Euler angles over time will be calculated by integrating their respective derivatives, which are calculated using the following equation, where p, q and r are the respective angular velocities in the body axis.

$$\begin{bmatrix} \dot{\phi} \\ \dot{\theta} \\ \dot{\psi} \end{bmatrix} = \begin{bmatrix} 1 & tan\theta sin\phi & tan\theta cos\phi \\ 0 & cos\phi & -sin\phi \\ 0 & sin\phi/cos\theta & cos\phi/cos\theta \end{bmatrix} \begin{bmatrix} p \\ q \\ r \end{bmatrix} \quad (2)$$

With the rotations between frames defined, navigation between reference points is possible by obtaining the position of the center of mass by integrating the aircraft's speed after converting its components into the NED frame.

$$\mathbf{p}_{CM}^{E} = \int \mathbf{C}_{Eb}\mathbf{v}_{CM/E}^{b} \quad (3)$$

Where $\mathbf{v}_{CM/E}^{b}$ is the speed of the center of mass in relation to the NED frame with components described in the body frame. Finally, it is important to include the speed of the incoming flow and wind and its relationship with the body's ground speed:

$$\mathbf{v}_{CM/E}^{b} = \mathbf{v}_{rel/E}^{b} + \mathbf{C}_{bE}\mathbf{v}_{wind/E}^{E} \quad (4)$$

Where $\mathbf{v}_{rel/E}$ the speed of the flow relative to the vehicle and $\mathbf{v}_{wind/E}^{E}$ the wind speed in relation to the NED frame with components described in the NED frame. If there is no wind, the airspeed will be equal to the aircraft speed in the body frame.

2.2. Dynamics

Using classical mechanics, the dynamics of the aircraft can be represented using a model of six degrees of freedom from the following vector equations, assuming that the NED frame is an inertial frame:

$$\dot{\mathbf{v}}_{CM/E}^{b} = \frac{\mathbf{f}_{T}^{b}}{m} - \mathbf{w}_{CM/E}^{b} \times \mathbf{v}_{CM/E}^{b} \quad (5)$$

$$\dot{\mathbf{w}}_{CM/E}^{b} = (\mathbf{I}^{b})^{-1}[\mathbf{m}_{T}^{b} - \mathbf{w}_{CM/E}^{b} \times \mathbf{I}^{b}\mathbf{w}_{CM/E}^{b}] \quad (6)$$

The sum of propulsion, aerodynamic and gravity forces and moments will result in the force vector $\mathbf{f}_{T}^{b} = \mathbf{f}_{g}^{b} + \mathbf{f}_{p}^{b} + \mathbf{f}_{a}^{b}$ and moment vector $\mathbf{m}_{T}^{b} = \mathbf{m}_{p}^{b} + \mathbf{m}_{a}^{b} + \mathbf{m}_{g}^{b}$ where the subscripts g, p and a stand for gravity, propulsion and aerodynamic forces or moments, respectively, which are discussed in the following subsections.

2.3. Gravity

The moment $\mathbf{M}_g$, present due to center of gravity displacement with respect to the center of mass, that for applications such as UAV motion control, this term is residual so it can be neglected. The force $\mathbf{f}_g$ can be easily defined in the NED coordinate frame with only a z component equal to the gravity constant of the earth at its surfaces times the mass of the object in question. The gravity force can then be described in the body frame using the transformation matrices defined before, resulting in the following equation:

$$\mathbf{f}_g^b = \mathbf{C}_{bE}\mathbf{f}_g^E = \mathbf{C}_{bE}\begin{bmatrix}0 & 0 & mg\end{bmatrix}^T \tag{7}$$

2.4. Propulsion

This section will address the model of the aircraft's propulsion, which includes four electric rotors(four motors + four propellers) that are powered by four batteries due to physical constraints. For each rotor, we will model a static response and a first order response with delay to model the transient response.

2.4.1. Static forces and moments

A propeller will transform rotational power into linear thrust by acting upon a fluid, such as air in this case. A given mass of the working fluid is accelerated in one direction and the craft moves in the opposite direction. Data retrieved from the propulsion test in the wind tunnel was used to model a static response of the rotor as a function of two inputs, the incoming airflow (u) and the input PWM signal (ms). This approach results on the graph in Figures 1(a)(b)(c), for the propeller with a diameter of 13 inches with an advance ratio of 8 inches per single revolution of the engine.

2.4.2. First order Transient Response

For the Transient Response, it is assumed an instantaneous response of torque and electrical power since its response is faster than the aircraft dynamics. Since the thrust depends directly on the rotor speed and it doesn't change as fast as the torque and energy do, we approximate the motor thrust transient response by a first order system with a certain time constant and a delay:

$$G(s) = \frac{Y(s)}{U(s)} = \frac{K}{K_T \cdot s + 1}e^{-t_d \cdot s} \tag{8}$$

which will correspond in the time domain to the following equation in this case:

$$\dot{T}(t) = \frac{K \cdot T_i(t - t_d) - T(t)}{K_T} \tag{9}$$

Where T is the Thrust and T_i is the steady-state value of the Thrust for a certain PWM input and incoming airflow (u), given by the propeller model,

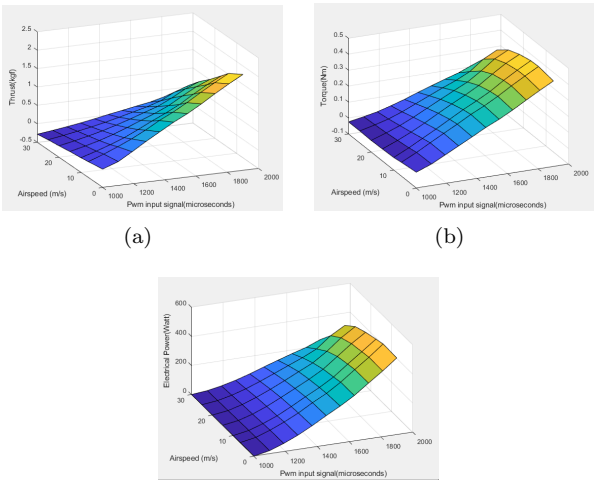

(a) (b) (c)

Figure 1: Rotor Static Response (a) Static Thrust (b) Static Torque and (c) Static Electrical Power measured of the propeller 13x8.

which serves as the input for the first order model. These values were obtained from the propulsion test, in which we determined that the rotor had a time constant of 0.078 s and a delay of 0.0576 s

From the individual forces and moments from each rotor produced at the propeller a translation from their position to the center of mass is done and the forces and moments exerted in the aircraft from the propulsion are obtained. Noting that in this UAV, all the four rotors are colinear with the x axis.

2.5. Aerodynamic

The work presented in the section is based on [5] [6] and [7], as a reference. First of all, two axes and two angles will have to be established to be used to describe these forces as a function of these variables, α and β.

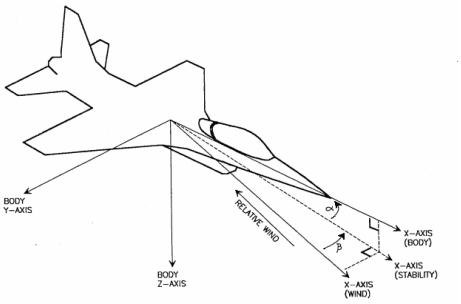

Figure 2: Definition of aerodynamic axis and angles.

An aircraft with a flow with a relative direction off center with the body axis is represented. By defining two new axis, the stability axis and wind axis, we define the angle of attack (α) as the angle

between the body's x-axis and the stability x-axis and the skid angle (β) the angle between the wind axis and the stability axis.

To obtain these variables, we assume that the components of the relative velocity of the airflow are defined as, $\mathbf{v}_{rel/E} = [U \quad V \quad W]$, in the body frame and so we are able to calculate these variables by using :

$$tan(\alpha) = \frac{W}{U}; \quad sin(\beta) = \frac{V}{|\mathbf{v}_{rel/E}|} \tag{10}$$

Defining the aerodynamic lift(L), drag(D) and lateral(Y) forces in the wind axis, we need to make a conversion to the body frame since it is in this axis that the dynamics of the aircraft is calculated and so using the rotation is necessary:

$$\mathbf{f}_A^b = \mathbf{C}_{bw} * \mathbf{f}_A^w; \quad \mathbf{f}_A^w = [-D \quad Y \quad -L]^T \tag{11}$$

These forces are functions of α, β, the deflections of the control surfaces, but also on the number of Mach and Reynolds, since the aircraft will fly at very low Mach numbers, its influence will be assumed to be negligible, on the other hand, the Reynolds number will depend on the flight condition assuming an operation between 15 m/s and 30 m/s corresponding to a Reynolds number around 340000 and 680000 (assuming air at room temperature of about 20 °). Additionally, these forces are defined according to their dimensionless aerodynamic coefficients, these aerodynamic coefficients are a function of the previous variables and the nondimensionalization is done using the dynamic pressure and a characteristic dimension of the aircraft depending on the force in question. To take some complexity out of the problem, we will assume that the aircraft works in the linear region, this simplification can be done with a reduced error for small angles, obtaining the following equations:

$$L = \left(C_{L_0} + C_{L_\alpha}\alpha + C_{L_q}Q\frac{c}{2V_{flow}} + C_{L_{\delta_e}}\delta_e + C_{L_{\delta_f}}\delta_f\right)\frac{\rho V_{flow}^2 S}{2} \tag{12}$$

$$D = \left(C_{D_0} + C_{D_\alpha}\alpha + C_{D_q}Q\frac{c}{2V_{flow}} + C_{D_{\delta_e}}\delta_e + C_{D_{\delta_f}}\delta_f\right)\frac{\rho V_{flow}^2 S}{2} \tag{13}$$

$$Y = \left(C_{Y_\beta}\beta + (C_{Y_p}P + C_{Y_r}R)\frac{b}{2V_{flow}} + C_{Y_{\delta_a}}\delta_a + C_{Y_{\delta_r}}\delta_r\right)\frac{\rho V_{flow}^2 S}{2} \tag{14}$$

The aerodynamic moments are defined in the body axes and are positive according to the right hand rule. As in the case of the aerodynamic forces, the aerodynamic moments are written as a function of their dimensionless aerodynamic coefficients that depend on the same variables and use the same assumptions and so we obtain the following expressions:

$$l = \left(C_{l_\beta}\beta + (C_{l_p}P + C_{l_r}R)\frac{b}{2V_{flow}} + C_{l_{\delta_a}}\delta_a + C_{l_{\delta_r}}\delta_r\right)\frac{\rho V_{flow}^2 Sb}{2} \tag{15}$$

$$m = \left(C_{m_0} + C_{m_\alpha}\alpha + (C_{m_q}Q)\frac{\bar{c}}{2V_{flow}} + C_{m_{\delta_e}}\delta_e + C_{m_{\delta_f}}\delta f\right)\frac{\rho V_{flow}^2 S\bar{c}}{2} \tag{16}$$

$$n = \left(C_{n_\beta}\beta + (C_{n_p}P + C_{n_r}R)\frac{b}{2V_{flow}} + C_{n_{\delta_a}}\delta_a + C_{n_{\delta_r}}\delta_r\right)\frac{\rho V_{flow}^2 Sb}{2} \tag{17}$$

3. Model Parameters

This section described how we found the aircraft parameters, showing information about dimensions, mass, inertia, aerodynamic coefficients, engine and propeller parameters. It will only focus on the UAV for which the control algorithms were designed, which is the F-02.

Figure 3: F-02 UAV

3.1. Center of mass

The correct location of the UAV center of mass (CM) and the measurement of the mass itself are essential for aircraft stability, a system, consisting of a four-point measurement system, is employed. In each of these points, a bar that contains a load cell is used to measure the weight. The UAV is placed on these load cells in a position such that the aircraft is upright. With the load information applied to each cell, it is possible then to directly determine the mass of the aircraft and estimate the location of its center of mass.

3.2. Moments of Inertia

The method of measurement of the moments of inertia of the prototypes, described in [8] [9] was used in this work, which consists of using a suspended structure to allow the free pendulum movement of the aircraft. Thus, the moments of inertia of the model can be obtained by measuring the periods of the pendulum oscillation around the various axes of rotation.

Table 1: Mass and center of mass measured values in relation to the leading edge and plane of symmetry.

Center of Mass properties			
UAV without fuselage		UAV without fuselage	
$m[Kg]$	6.409	$m[Kg]$	7.435
$g[m/s^2]$	9.806	$g[m/s^2]$	9.806
$X_{cg}[m]$	-0.094	$X_{cg}[m]$	-0.089
$Y_{cg}[m]$	0.000	$Y_{cg}[m]$	0.000
$Z_{cg}[m]$	0.003	$Z_{cg}[m]$	0.016

Table 2: Summary of the inertia parameters necessary for the 6 degree freedom dynamics model.

Inertia Parameters			
UAV without fuselage		UAV without fuselage	
$I_{xx}[Kgm^2]$	0.782	$I_{xx}[Kgm^2]$	0.798
$I_{yy}[Kgm^2]$	0.218	$I_{yy}[Kgm^2]$	0.307
$I_{zz}[Kgm^2]$	1.070	$I_{zz}[Kgm^2]$	1.107
$I_{xy}, I_{yx}[Kgm^2]$	0.000	$I_{xy}, I_{yx}[Kgm^2]$	0.000
$I_{xz}, I_{zx}[Kgm^2]$	0.024	$I_{xz}, I_{zx}[Kgm^2]$	0.275
$I_{yz}, I_{zy}[Kgm^2]$	0.000	$I_{yz}, I_{zy}[Kgm^2]$	0.000

Noting that the aircraft has a plane of symmetry, so the products of inertia I_{xy} and I_{yz} can be neglected. And the product of inertia I_{xz} follows a similar procedure to the one used for the determination of the moment of inertia around the x axis but with an added inclination to the oscillations to make it possible to measure the product of inertia I_{xz}.

3.3. Aerodynamic Coefficients

Due to difficulties and the lack of equipment to directly measure all the necessary aerodynamics parameters in the wind tunnel, we need to estimate them using computational tools, in this case, using XFLR5 software. XFLR5 results need to be considered preliminary and experimental but have shown promise and some precision especially for longitudinal variables and slow periodic modes [10] [11].

Additionally, we need a way to add the influence on the aerodynamics from the landing gear and the detachable fuselage. Unfortunately, the XFRL5 does not recommend adding these components directly in the analysis and instead recommends adding them as an extra drag coefficient ($C_{D_{0fus}}$ $C_{D_{0gear}}$) with their respective frontal area.

In the case of the landing gear, equation 2.49 allows us to obtain a rough estimate of the value of the aerodynamic resistance coefficient caused by their presence and for the fuselage, we are able to get a drag coefficient from [12].

$$C_{D_{0gear}} = 3.23\sqrt{MTOW}\frac{A_{gear}}{S} \tag{18}$$

Table 3: Fuselage values and landing gear data

Fuselage		Landing Gear (1:10)			
$C_{D_{0fus}}$	A_f $[m^2]$	MTOW $[kg]$	$A_{gear}[m^2]$	S$[m^2]$	$C_{D_{0gear}}$
0.005	0.025	6.409	0.005	0.358	0.114

After defining all the necessary inputs and creating the required airfoil Polars, we can use XFRL5 stability analysis to estimate the aerodynamic coefficients for the entire aircraft and present them separately for the longitudinal dynamics and for the lateral dynamics in the following table.

Table 4: Aerodynamics derivatives for the longitudinal and lateral dynamics.

Longitudinal aerodynamics derivatives			Lateral aerodynamics derivatives		
Symbol	Value	Value (with fuselage)	Symbol	Value	Value (with fuselage)
C_{L_0}	0.215	0.215	C_{Y_β}	-0.359	-0.386
C_{L_α}	4.804	4.804	C_{Y_p}	0.000	0.000
C_{L_q}	7.993	8.0577	C_{Y_r}	0.345	0.352
$C_{L_{\delta_e}}$	0.389	0.389	$C_{Y_{\delta_a}}$	0.029	0.029
$C_{L_{\delta_f}}$	0.535	0.538	$C_{Y_{\delta_r}}$	0.198	0.198
C_{D_0}	0.015	0.015	C_{l_β}	-0.040	-0.039
C_{D_α}	0.052	0.052	C_{l_p}	-0.420	-0.420
C_{D_q}	0.000	0.000	C_{l_r}	0.126	0.133
$C_{D_{\delta_e}}$	0.036	0.036	$C_{l_{\delta_a}}$	-0.229	-0.229
$C_{D_{\delta_f}}$	0.0165	0.0165	$C_{l_{\delta_r}}$	0.009	0.011
C_{m_0}	0.007	0.003	C_{n_β}	0.158	0.159
C_{m_α}	-0.741	-0.8634	C_{n_p}	-0.096	-0.096
C_{m_q}	-15.330	-15.538	C_{n_r}	-0.155	-0.1625
$C_{m_{\delta_e}}$	-1.283	-1.292	$C_{n_{\delta_a}}$	-0.014	-0.014
$C_{m_{\delta_f}}$	-0.055	-0.0645	$C_{n_{\delta_r}}$	-0.098	-0.099

3.4. Propulsion parameters

To characterise the behaviour of the rotor that includes the electric motor, ESC and the propeller, the propulsion system was installed on a test bench (see Figure 4), and an external structure of the test bench was designed to accommodate the acquired test bench (from RCbenchmark) in the right place in the wind tunnel. This test bench can control the signal sent to the ESC that controls the speed of the motor and acquires the data from the load cells and optical sensor. Finally, since the wind tunnel is already calibrated, we can know the speed of the flow that approaches our electric rotor.

The propellers are identified by their diameter and pitch, and here we used a 13x8 propeller. With this test setup, several parameters can be measured and recorded in tables 5, 6 and 7 for the propeller 13x8.

One other aspect we want to study in this section is the time response of the rotor. To do so, we study the response to step inputs and, with this information, we can model its transient response to a possible first order system. It is observed that the thrust time response is clearly different from the torque and electric power time response, which

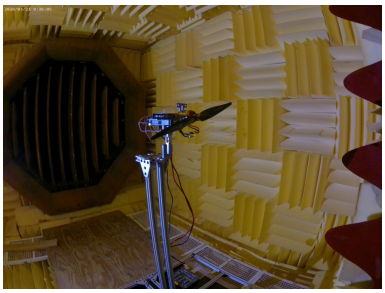

Figure 4: Propulsive test bench in the IST acoustic wind tunnel

Table 5: Rotor Static Thrust Response measured of the propeller 13x8.

Thrust(kgf) 13x8	Incoming Airflow Velocity (m/s)						
PWM(μs)	0.00	6.60	10.01	15.02	20.00	25.02	30.10
1000	0	-0.06787	-0.1013	-0.1373	-0.1886	-0.2288	-0.2828
1100	0.15296	0.086007	0.027432	-0.038081	-0.10351	-0.16205	-0.23056
1189	0.37428	0.23988	0.15613	0.061122	-0.01841	-0.095267	-0.17832
1278	0.6077	0.40637	0.29824	0.18314	0.075412	-0.025235	-0.12134
1367	0.82388	0.59912	0.47314	0.32205	0.18519	0.055236	-0.055823
1456	1.0397	0.81368	0.65854	0.47105	0.30247	0.14637	0.016291
1544	1.2246	0.99442	0.82783	0.61385	0.42985	0.24056	0.080475
1633	1.4419	1.2075	1.0164	0.77999	0.55413	0.33531	0.14939
1722	1.6777	1.4398	1.2493	0.99685	0.73471	0.45371	0.21315
1811	1.898	1.6557	1.4633	1.2002	0.93945	0.64595	0.30588
1900	2.1055	1.8623	1.6535	1.3568	1.0916	0.77754	0.28454

Table 6: Rotor Static Torque Response measured of the propeller 13x8.

Torque (Nm) 13x8	Incoming Airflow Velocity (m/s)						
PWM(μs)	0.00	6.60	10.01	15.02	20.00	25.02	30.10
1000	0	-0.01252	-0.02107	-0.02426	-0.02697	-0.02436	-0.02429
1100	0.036353	0.03439	0.024656	0.014415	0.0052805	-0.0011942	-0.0068808
1189	0.079641	0.081304	0.070379	0.053093	0.037533	0.021973	0.010532
1278	0.12291	0.12681	0.11519	0.096407	0.076223	0.053532	0.034801
1367	0.16649	0.17122	0.16291	0.14399	0.11919	0.090521	0.061248
1456	0.21149	0.21859	0.20985	0.18935	0.16173	0.12738	0.092174
1544	0.24976	0.25918	0.25197	0.23158	0.20309	0.16358	0.11979
1633	0.29439	0.3057	0.29764	0.2783	0.24347	0.19751	0.14797
1722	0.34327	0.35758	0.35331	0.33623	0.29949	0.23821	0.17395
1811	0.39074	0.40573	0.40382	0.3903	0.3615	0.30294	0.20905
1900	0.43588	0.45238	0.45019	0.43279	0.40421	0.34685	0.19924

Table 7: Rotor Static Electrical Power Response measured of the propeller 13x8.

Power (Watt) 13x8	Incoming Airflow Velocity (m/s)						
PWM(μs)	0.00	6.60	10.01	15.02	20.00	25.02	30.10
1000	0	0	0	0	0	0	0
1100	21.4672	19.9531	19.2394	16.8646	14.5043	12.2982	10.0494
1189	56.6002	54.4286	51.3402	45.6742	41.2333	34.2203	28.0516
1278	98.2824	95.7419	90.2141	84.109	75.9916	63.9796	51.756
1367	148.214	142.9421	138.8774	130.1416	116.963	100.1281	80.8096
1456	202.9577	198.8391	191.3995	177.9878	161.5161	139.427	113.9781
1544	254.2345	248.2563	240.7791	226.2572	207.9063	178.8974	145.1783
1633	312.0449	310.4816	298.0831	280.7677	253.8412	218.4812	175.7908
1722	382.5936	382.4213	371.6216	353.7039	318.8438	263.9148	204.2415
1811	451.001	452.3811	442.5443	426.6805	396.4776	340.3274	242.85
1900	526.0878	528.9071	514.1841	490.0816	458.9158	396.0695	227.5342

have faster responses. Therefore, we represent our torque and electric power time response as instantaneous. For the thrust, two candidates were assumed as appropriate candidates: a first order system with no delay and a first order system with a delay (since they were a good compromise between accuracy and simplicity), thus achieving the following results given in figure 5.

The model that provides the best fit to transient

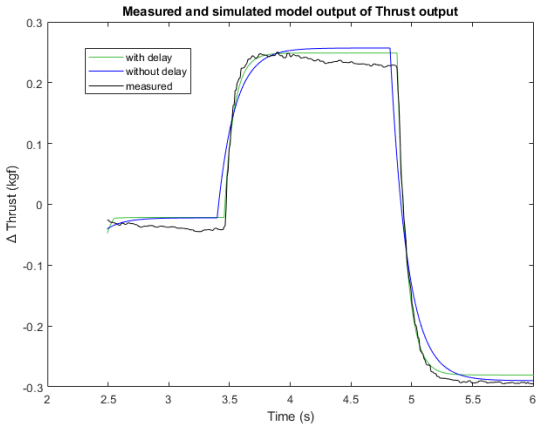

Figure 5: Rotor Modelled Thrust Transient Response versus Measured

response is the one with the delay and so we can conclude this section by assuming a first order system with a pole at -12.81 and a delay of 0.0576 seconds.

4. Linear Control

This chapter describes the linear control design techniques that are going to be employed in this project. To do so, we need first to derive a linear model from the derived nonlinear model in the previous section by linearizing said model around a trimming flight condition which is dependent on its airspeed. We will take advantage of this dependency to create an airspeed gain scheduling, a design approach that constructs a nonlinear controller for a nonlinear plant by patching together a collection of linear controllers.

5. Steady-State Trimming

By trimming the model we reach a certain flight condition where that linearization can be performed. This flight condition will be defined as a state where the aircraft maintains a steady wing levelled flight, which leads to constant forces and moments in the body-fixed coordinate system, with fixed controls making α, β and angular angles also constant, and therefore their derivatives equal to zero and so we can draw the following conditions, at a constant altitude and velocity, V_T: .

$$\begin{bmatrix} U = V_T cos(\alpha) cos(\beta) \\ V = V_T sin(\beta) \\ W = V_T sin(\alpha) cos(\beta) \end{bmatrix} \begin{bmatrix} P = 0 \\ Q = 0 \\ R = 0 \end{bmatrix} \begin{bmatrix} \psi = 0 \\ \theta = ? \\ \phi = * \end{bmatrix} \begin{bmatrix} N = * \\ E = * \\ D = * \end{bmatrix} \tag{19}$$

$$\begin{bmatrix} \dot{U} = 0 \\ \dot{V} = 0 \\ \dot{W} = 0 \end{bmatrix} \begin{bmatrix} \dot{P} = 0 \\ \dot{Q} = 0 \\ \dot{R} = 0 \end{bmatrix} \begin{bmatrix} \dot{\psi} = 0 \\ \dot{\theta} = 0 \\ \dot{\phi} = 0 \end{bmatrix} \begin{bmatrix} \dot{N} = * \\ \dot{E} = * \\ \dot{D} = 0 \end{bmatrix} \tag{20}$$

Where, (*) indicates that any value is inside the flight envelope is possible to be used and (?) indicates a trim variable. Furthermore we need to trim the input vector, where δ_e, δ_a, δ_r, δ_{T1}, δ_{T2}, δ_{T3}, δ_{T4}, are trim inputs and δ_f can be imposed depending in the flight phase. The values for the airspeed (V_T) will differ depending on the flight phase, so we will make several linearizations between the take-off speed and the maximum speed (30 m/s).

With the conditions defined in 19 and 20, we can perform an algebraic trim that will be used in the numerical trim in the next section as initial input for this numerical trim. This algebraic can be obtained from the longitudinal mode using equations 21, 22 and 23.

$$C_{m_0} + C_{m_\alpha}\alpha + C_{m_{\delta_e}}\delta_e + C_{m_{\delta_f}}\delta_f + C_{m_{\delta_{fa}}}\delta_{fa} = 0 \tag{21}$$

$$-mg\sin\alpha - D\cos\alpha + L\sin\alpha + T = 0 \tag{22}$$

$$mg\cos\alpha - L\cos\alpha + D\sin\alpha = 0 \tag{23}$$

where:

$$L = (C_{L_0} + C_{L_\alpha}\alpha + C_{L_{\delta_e}}\delta_e + C_{L_{\delta_f}}\delta_f)\frac{\rho V_T^2 S}{2} \tag{24}$$

$$D = (C_{D_0} + C_{D_\alpha}\alpha + C_{D_{\delta_e}}\delta_e + C_{D_{\delta_f}}\delta_f)\frac{\rho V_T^2 S}{2} \tag{25}$$

Since δ_f values are predefined, we can obtain the variables θ, δ_e and T in table 8 for the UAV without fuselage and table 9 for the UAV with the fuselage.

Table 8: Steady-state flight algebraic trim results for the UAV without the fuselage.

V_T [m/s]	δ_f[°]	U [m/s]	W [m/s]	θ [°]	δ_e[°]	T[N]
17.145	0	16.915	2.796	9.3849	-5.1193	4.198
16.091	20	16.091	2.457	8.7825	-5.6225	3.710
20	0	19.882	2.166	6.2182	-3.2903	3.657
25	0	24.965	1.318	3.0213	-1.4440	3.546
30	0	29.993	0.667	1.2747	-0.4352	4.039

Table 9: Steady-state flight algebraic trim results for the UAV with the fuselage.

V_T [m/s]	δ_f[°]	U [m/s]	W [m/s]	θ [°]	δ_e[°]	T[N]
18.467	0	18.215	3.039	9.471	-6.197	4.908
17.331	20	17.124	2.674	8.8755	-6.7979	4.333
20	0	19.819	2.681	7.7024	-5.0155	4.521
25	0	24.939	1.735	3.9792	-2.5275	4.093
30	0	29.983	1.016	1.9402	-1.1648	4.429

We can also trim the nonlinear model numerically using the tools available in MATLAB/SIMULINK simulation environment and calculate the values of all variables in the trim conditions. This numerical trim consists of a non-linear minimisation problem, starting from an initial point provided by the algebraic trim done before and it searches using a sequential quadratic programming algorithm (SQP) [13], until it finds the nearest trim point. These values are similar to the values found in the algebraic trim and so we can be assured that this step is done correctly.

5.1. Model Linearization

To linearize the non-linear model, we need to determine a set of first order differential equations, that represent the system around the steady state condition and where a numerical method is used with the tools available in MATLAB with the routine *linearize*. The aircraft equations can be written as a continuous-time state-space mode resulting in the following state equation 26 and output equation 27:

$$\dot{\mathbf{X}} = f(\mathbf{X}, \mathbf{U}, \mathbf{W}) \quad \mathbf{X}(n \times 1), \quad \mathbf{U}(m \times 1) \tag{26}$$

$$\mathbf{Y} = g(X, U), \quad \mathbf{Y}(n \times 1) \tag{27}$$

With the equations 26, 27 and considering a steady-state trimmed flight condition, we can expand these non-linear state equations in a Taylor series about the equilibrium point ($\mathbf{X}_T$, $\mathbf{U}_T$), keeping only the first order term, yielding

$$\begin{aligned} f(\mathbf{X}, \mathbf{U}) &= f(\mathbf{X}_T, \mathbf{U}_T) + \frac{\partial f}{\partial X}(\mathbf{X} - \mathbf{X}_T)\frac{\partial f}{\partial \mathbf{U}}(\mathbf{U} - \mathbf{U}_T) \\ &= \mathbf{A}(\mathbf{X} - \mathbf{X}_T) + \mathbf{B}(\mathbf{U} - \mathbf{U}_T) \end{aligned} \tag{28}$$

With the partial derivatives numerically approximated by:

$$\frac{\partial f}{\partial \mathbf{X}} = \frac{f(\mathbf{X}_T + \mathbf{x}_i, \mathbf{U}_T) - f(\mathbf{X}_T, \mathbf{U}_T)}{\mathbf{x}_i} \tag{29}$$

$$\frac{\partial f}{\partial \mathbf{U}} = \frac{f(\mathbf{X}_T, \mathbf{U}_T + \mathbf{u}_i) - f(\mathbf{X}_T, \mathbf{U}_T)}{\mathbf{u}i} \tag{30}$$

5.2. Longitudinal modes

From the matrices obtained before we can extract the longitudinal modes by considering the state vector, $\mathbf{X} = [u, w, q, \theta]$, and input vector, $\mathbf{U} = [\delta_e, \delta_T]$, since the coupling modes are residual and with the rotor dynamics simplified to an instantaneous thrust response. For example for a speed of 30 m/s we obtain

$$\mathbf{A}_{long} = \begin{bmatrix} -0.2402 & 0.2658 & -0.6447 & -9.8036 \\ -0.543 & -4.9495 & 28.9750 & -0.2181 \\ 0.2389 & -5.6416 & -14.7770 & 0 \\ 0 & 0 & 1 & 0 \end{bmatrix} \tag{31}$$

$$\mathbf{B}_{long} = \begin{bmatrix} -0.849 & 4.736 \\ -11.977 & 0 \\ -293.423 & -2.158 \\ 0 & 0 \end{bmatrix} \tag{32}$$

And using damp, MATLAB routine, we can display the damping ratio, natural frequency and poles of the linear model, shown in Table 10. We can see that all eigenvalues are complex numbers with negative real parts and so the aircraft is said to be dynamically stable. Also, the lowest frequency pole is associated with the phugoid mode and the other pair is associated with the short period.

Table 10: Longitudinal mode poles

Poles	Damping	Frequency(rad/s)
-0.122+4i	0.291	4.180
-0.122-4i	0.291	4.180
-9.862+11.808i	0.641	15.385
-9.862-11.808i	0.641	15.385

5.3. Lateral modes

The lateral modes will consider the following state vector, $\mathbf{X} = [v, p, r, \phi, \psi]$, and input vector $\mathbf{U} = [\delta_a, \delta_r]$ for the lateral modes and with the same assumptions made for the longitudinal mode, we can obtain the following matrices, for a speed of 30 m/s:

$$\mathbf{A}_{lat} = \begin{bmatrix} -0.389 & 0.668 & -29.745 & 9.804 & 0 \\ -0.595 & -3.926 & 1.2567 & 0 & 0 \\ 1.455 & -0.637 & -1.077 & 0 & 0 \\ 0 & 1 & 0.022 & 0 & 0 \\ 0 & 0 & 1.0002 & 0 & 0 \end{bmatrix} \tag{33}$$

$$\mathbf{B}_{lat} = \begin{bmatrix} 0.882 & 6.090 \\ -86.305 & 5.015 \\ -3.323 & -27.146 \\ 0 & 0 \\ 0 & 0 \end{bmatrix} \tag{34}$$

Using again the MATLAB routine damp, we can display the damping ratio, natural frequency and poles of the linear model, shown in Table 11. We can see that most eigenvalues are real and negative, or complex with negative real parts except for a pole in the origin which corresponds to the integration of the yaw rate and a positive real pole that correspond to the spiral that is unstable, as usual in most aircraft. The lowest frequency real pole is associated with the roll mode and the other pair of complex poles are associated with the dutch roll.

Table 11: Lateral mode poles

Poles	Damping	Frequency(rad/s)
0	-1	0
0.0678	-1	0.068
-4.187	1	4.187
-0.636+6.729i	0.094	6.759
-0.636-6.729i	0.094	6.759

6. Proposed Controller

With the Pixhawk board Controller, we could not find a solution that provided a stabilisation of the spiral mode with the presence of the washout-filter in the yaw controller with a cut-off frequency of 0.2 rad/s that would slowly create an instability since in this aircraft the spiral mode is naturally unstable. And so we propose a classical controller that uses a cascaded-loop architecture with three inner P-only loops with feedback of the angular rates p,q,r to stabilise the UAV, and two outer PI loops to control the θ and ϕ orientation angles, making compatible with the existing position controllers of the Pixhawk board. This five proportional gains and two integral gains are all scheduled as a function of flight velocity.

6.1. Angular Rate Control

The three inner loops are used to stabilise the UAV and their control laws are expressed in equations 35,36 and 37.

$$\delta_r = K_r(\dot{\psi}_{ref} + \dot{\psi}) \tag{35}$$

$$\delta_a = K_p(\dot{\phi}_{ref} - \dot{\phi}) \tag{36}$$

$$\delta_e = K_q(\dot{\theta}_{ref} + \dot{\theta}) \tag{37}$$

The influence of the gains K_r, K_p and K_q are analysed using the root-locus technique, that generate the poles locations, as a function of these gains. As a result of this graphical method, along with the poles of the closed loop for this particular values of $K_r = 0.361$, $K_p = 0.0176$ and $K_q = 0.036$ are in table 12 for the lateral dynamic modes and in table 13 for the longitudinal dynamic modes. In terms of lateral dynamics, these gains make the pole associated with the spiral mode stable since it is now in the left side of the complex plane at the same time increasing the damping and frequency of the dutch roll mode and decreasing the frequency of the roll mode but still over 1 rad/s, from the lateral criteria in [14], we can confirm that the UAV still flies in the level 1.

Table 12: Lateral modes poles of the closed loop of the inner loop.

Poles	Damping	Frequency(rad/s)
0	1	0
-0.2792	1	0.279
-2.0315	1	2.032
-6.336-0.1.685i	0.97	6.560
-6.336+0.1.685i	0.97	6.560

Table 13: Longitudinal mode poles of the closed loop of the inner loop.

Poles	Damping	Frequency(rad/s)
-0.1241+0.395i	0.327	0.380
-0.1241-0.395i	0.327	0.380
-15.661+6.792i	0.917	17.010
-15.661-6.792i	0.917	17.010

In terms of longitudinal dynamics, this gain value was chosen in order to increase the damping of the longitudinal modes and from the longitudinal criteria in [14], we can confirm that the UAV still flies in the level 1. For all conditions the gains vectors calculated are in equations 38, 39, 40:

$$K_r = [0.679 \quad 0.586 \quad 0.423 \quad 0.361] \tag{38}$$

$$K_p = [0.034 \quad 0.321 \quad 0.0221 \quad 0.0176] \tag{39}$$

$$K_q = [0.0638 \quad 0.0459 \quad 0.0395 \quad 0.036] \tag{40}$$

6.2. Attitude Control

We will now focus on the two gain-scheduled PI loops controlling roll and pitch angles. These outer loops are given by the following control laws:

$$p_{demand} = K_\phi(\phi_{ref} + \phi) + I_\phi \int (\phi_{ref} + \phi)dt \tag{41}$$

$$q_{demand} = K_\theta(\theta_{ref} + \theta) + I_\theta \int (\theta_{ref} + \theta)dt \tag{42}$$

These loops are tuned for each flight condition using the MATLAB routine *systune* to tune the PI gains for specific goals, in this case a phase margin of 40 dB, a gain margin of 6 db and a target time response between 3 and 30 seconds.

To tune the outer loops, we close the inner loops and obtain a linearized model of the plant seen by the outer loops, but to get the correct linearization, we set tuner in such a way that the inner loop gains vary with flight velocity and this possible with block

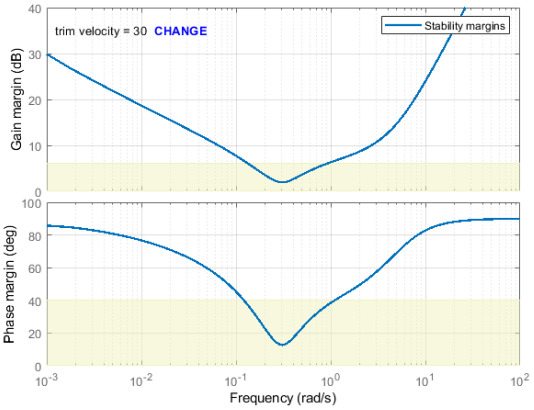

Figure 6: Stability Analysis Using Gain and Phase Disk Margins.

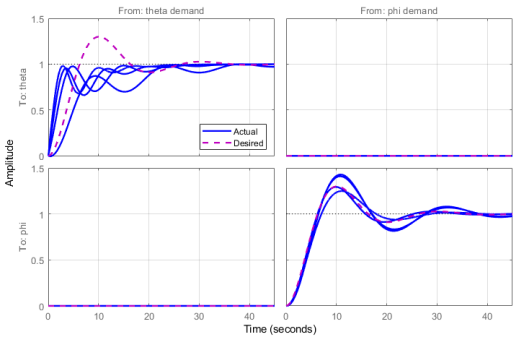

Figure 7: Obtained system time response.

substitution in the SIMULINK enviroment. After the automated tuning we achieve the following results:

We can conclude that the system can't reach an adequate phase and gain disk margins around 0.3 rad/s, even with a relaxed target for the time response. And so we have to conclude that the controller design did not accomplish all its goals since it does not provide the target stability and at the same time its time response is quite slow.

7. Conclusions

The main reason to build this scaled aircraft was to draw some conclusions about the viability of this configuration for the specified mission. In that account, we have to come to terms that there is a need to revise or even change the aircraft configuration. The main drawback, from the current choice, comes down to the struggle to position the center of mass without adding a lot of dead weight on the foreside of the wing or reducing so much weight on the tail structure that it compromises its rigidity. The possibility of a flight without a fuselage makes it harder to position the center of mass in a place that provides greater stability for this configuration. A possible solution to this problem may be found

in changing the configuration to a tandem wing, which does not come without its own issues; still, it definitely gives more freedom when it comes to the center of mass location with or without the fuselage.

A computational model of the scaled model was made, containing the aircraft forces, moments, navigation, and cinematic differential equations, with this model, it is possible to test several missions and flight conditions, while at the same time, help design the controllers for the UAV in question. This last task was partially accomplished. While a control algorithm is designed, it is still a simple control, and there is still much work to be done in this area. In the end the controller did not achieve a desirable fast time response and work still has to be done to improve this controller. Additionally, a position controller still needs to be done to provide full autonomous flight capabilities.

Finally, several experimental tests were performed to measure several parameters directly on the UAV. The inertia tests are used to obtain the inertia matrix with and without fuselage, and were performed with success. The location of the center of mass was determined with the use of several load cells, an essential parameter to assure stability. Furthermore, with the acquisition of a propulsion test rig and the use of the wind tunnel, the rotor behaviour was modelled with success.

Lastly, a flight was performed. Unfortunately, the results weren't optimistic, and it was found that the longitudinal modes were most likely unstable from the pilot input and the data recorded.

7.1. Future Work

From this work, one can envision further research activities which could result in full autonomous flight of the scaled model. First of all, increase the rigidity of the tail structure to improve flight qualities. One way of doing this is by adding rigging wires to the structure. Estimate the parameters again, this time based on flight data obtained from remotely piloted flights, to validate the obtained computational model by performing experimental fight tests in open loop. After this parameter identification task, we may improve the controller model of the PID loops, correct the control strategies for the new estimated parameters and check the nonlinear model behaviour in the presence of wind and wind gusts. Finally, we may test the controller by uploading it to the Pixhawk board and tested it in an actual flight.

References

[1] NASA J.Chambers. *Modeling flight : the role of dynamically scaled free-flight models in support of NASA's aerospace programs.* U.S Government Printing Office, 07 2016.

[2] SETsa. Flexcraft - modular, stol, flexível, 2019. URL `http://flexcraft.pt/en/consortium_en/` Last accessed:2020-11-29.

[3] R. Reis, M. Quintiães, and M. Rodrigues. Estudos preliminares - contexto de operação, mercado e certificação. Technical report, Flexcraft Consortium, 04 2017. PROJECTO No 17805.

[4] J. Vale, F. Afonso, A. Suleman, and F. Lau. Estudos preliminares - estudo de configuração de aeronaves. Technical report, Flexcraft Consortium, 04 2017. PROJECTO No 17805.

[5] J. D. Anderson. *Introduction to flight (4th ed.).* New York, NY: McGraw-Hill., 07 1999.

[6] B. Etkin and L. D. Reid. *Dynamics of Flight - Stability and Control.* John Wiley and Sons, Inc., 07 1996.

[7] Brian L Stevens and Frank L Lewis. *Aircraft Control and Simulation (2nd ed.).* John Wiley and Sons, Inc., 07 2003.

[8] C. M. M. Vilchez F. L. de Silva Bussamra and J. C. Santos. Experimental determination of unmanned aircraft inertial properties. In *ITA – Instituto Tecnológico de Aeronáutica - 2009 Brazilian Symposium on Aerospace Eng. and Applications*, 2009.

[9] Miller M. P. An accurate method of measuring the moments of inertia. Technical report, Langley Memorial Aeronautical Laboratory, 10 1930. No. 351.

[10] A. Deperrois. About xflr5 calculations and experimental measurements, 2009. URL `http://www.xflr5.tech/docs/Results_vs_Prediction.pdf` Last accessed: 2021-02-19.

[11] A. Deperrois. Modal analysis and experimental validation, 2011. URL `http://www.xflr5.tech/docs/XFLR5_Mode_Measurements.pdf` Last accessed:2021-02-19.

[12] H. Policarpo, F. Afonso, A. Suleman, and F. Lau. Projecto de vrp. Technical report, Flexcraft Consortium, 09 2018. PROJECTO No 17805.

[13] MATLAB. trim. URL `https://www.mathworks.com/help/simulink/slref/trim.html` Last accessed:2021-07-5.

[14] J. R Azinheira. Folhas da cadeira de controlo de voo, 2016.